JGR Atmospheres

RESEARCH ARTICLE
10.1029/2019JD032024

Special Section:
A NEW ERA OF LIGHTNING OBSERVATIONS FROM SPACE

Time Evolution of Satellite-Based Optical Properties in Lightning Flashes, and its Impact on GLM Flash Detection

Daile Zhang[1] and Kenneth L. Cummins[2]

[1]Earth System Science Interdisciplinary Center, University of Maryland, College Park, MD, USA, [2]Department of Hydrology and Atmospheric Sciences, University of Arizona, Tucson, AZ, USA

Key Points:

- The Geostationary Lightning Mapper detection efficiency increases with increasing flash duration and is highest for cloud-to-ground flashes
- Nearly half of the sources reported by the Lightning Imaging Sensor were less than 1/4th the size of a Geostationary Lightning Mapper pixel
- For small sources, the cloud-top energy threshold for the Geostationary Lightning Mapper is higher than for the Lightning Imaging Sensor

Correspondence to:
D. Zhang,
dlzhang@email.arizona.edu

Citation:
Zhang, D., & Cummins, K. L. (2020). Time evolution of satellite-based optical properties in lightning flashes, and its impact on GLM flash detection. *Journal of Geophysical Research: Atmospheres*, *125*, e2019JD032024. https://doi.org/10.1029/2019JD032024

Received 8 NOV 2019
Accepted 2 MAR 2020
Accepted article online 5 MAR 2020

Abstract The GOES-16 Geostationary Lightning Mapper (GLM) detection efficiency (DE) is studied over a full year (2018/19) in central Florida using the Kennedy Space Center Lightning Mapping Array (KSC LMA). Mean daily flash DE was 73.8%, and detection was highest during nighttime hours. GLM reported 86.5% of the LMA flashes that had coincident cloud-to-ground return strokes reported by the U.S. National Lightning Detection Network. Results also reveal that flash size and duration are critical parameters influencing GLM detection, regardless of the storm type, with 20–40% detection for small and short-duration flashes and greater than 95% detection for very large and long-duration flashes.
These findings can be explained by examining the time-evolution of cloud-top optical emissions observed by the Lightning Imaging Sensor (LIS). Statistical simulations based on long-term LIS group area observations indicate that about half of the above-threshold light sources are smaller than a LIS pixel (~ 4 × 4 km) and are smallest during and just after an initial breakdown in IC flashes. This work also demonstrates that for sources smaller than a GLM pixel, the cloud-top energy detection threshold for GLM is double that for LIS despite GLM's lower energy density threshold. Overall, these findings provide a framework for interpreting GLM performance under varying meteorological conditions, and help explain reports of low flash detection efficiency for storms associated with severe weather, as they typically exhibit high flash rates and resulting small and short-duration flashes.

Plain Language Summary The Geostationary Lightning Mapper (GLM) on the GOES-16 satellite is the first of a new generation of satellite-based optical lightning sensor. It is the first satellite sensor to detect the evolution of lightning activity throughout the lifecycle of thunderstorms, and the data products can provide a lead-time for improving severe weather nowcasting such as tornados, strong winds, and large hail. During 2017–2018, GLM detected more than 70% of all lightning flashes in central Florida. The GLM-detected flashes typically last longer and occupy larger areas. Data from the Lightning Imaging Sensor (LIS) and modeling results indicate that longer-duration flashes tend to produce brighter and larger light sources for GLM to detect, whereas shorter-duration flashes tend to produce dimmer and smaller light sources that the GLM might not detect. This finding furthers our understanding of the underlying GLM detection behaviors and will help improve how GLM products are used in severe weather forecasting and other applications.

1. Introduction

Since the launch of the GOES-16 and GOES-17 satellites, each with a state-of-art Geostationary Lightning Mapper (GLM) onboard, lightning observation from space has taken a giant leap. Their ability to continuously observe and collect lightning data at fixed positions is of great importance for studying the lifecycle of thunderstorms, and therefore, improving storm forecasting and nowcasting. Early assessments of GLM indicate that it exceeds the design specification of 70% flash detection efficiency (Goodman et al., 2013) when averaged over full days across the full domain (Koshak et al., 2018). However, some studies during instrument validation (Hilburn et al., 2019; Marchand et al., 2019; Thomas et al., 2019) indicate that GLM had much lower detection efficiencies for storms that produce low-altitude flashes (frequently referred to as inverted-polarity storms), severe storms when the flash rate was high, and/or when the flashes were small.

The GLMs were expected to have a higher detection efficiency for intra-cloud (IC) flashes than cloud-to-ground (CG) flashes, similar to findings from the Lightning Imaging Sensor (LIS) onboard the

low Earth orbital Tropical Rainfall Measuring Mission (TRMM) satellite (Franklin, 2013; Thomas et al., 2000). This is because IC flashes are expected to include more channels in the upper portions of the cloud than CG flashes which initiate and propagate more frequently in the lower portions of the cloud. It is also consistent with the modeling results by Thomason and Krider (1982). However, early assessment studies have shown that the GLMs have a higher detection efficiency for CG flashes than IC flashes (Bitzer, 2019; Yoshida, 2019). The so-called hybrid flashes with extensive IC components as well as connections to ground complicate this interpretation and may sometimes be as common as CG flashes that exclusively have channels in the lower part of the cloud (Mecikalski et al., 2017; Mecikalski & Carey, 2018).

The present study introduces a new way of examining GLM flash detection as a function of time evolution in the flash. We first show the detection efficiencies of GLM as a function of flash parameters (i.e. flash duration, channel length, etc.) derived using the very high frequency (VHF) Lightning Mapping Array (LMA) at the Kennedy Space Center (KSC) in Florida, USA. To help explain why GLM exhibits lower detection efficiency for spatially small and temporally short flashes, we evaluate the time-evolution of cloud-top optical parameters throughout the flash lifecycle using long-term datasets produced by TRMM LIS. These findings are then related to the dependence of GLM detection on flash size/duration, determined using the KSC LMA dataset.

2. Instruments and Methods

2.1. Geostationary Lightning Mappers (GLM)

After an initial 9 months of post-launch test and validation, the new generation of satellite-based lightning sensors (GLMs) are now in operational use to provide real-time lightning observations for tracking storms and assisting in storm forecasting (Goodman et al., 2013). Currently, the two GLMs are onboard the GOES-16 (centered at 75° W) and − 17 (137° W) satellites, with a latitude coverage of ±54° (Rudlosky et al., 2019). GLMs are designed to measure cloud-top radiation signatures at 777.4 nm (with a 1 nm bandwidth) produced by transient lightning discharges in both IC and CG flashes. These sensors have a wide field-of-view (FOV) with 1372 × 1300 pixels in the Charge Coupled Device (CCD) array at the focal plane (Goodman et al., 2013). The GLM pixel size varies throughout the field of view, from ~8 km at nadir to ~14 km at the edge of the field of view.

The GLM sensors capture images above the clouds at approximately 500 frames per second. Illumination on each pixel is accumulated during this 2 ms period and then sent to real-time event processors for determination of dynamic background illumination and subsequent processing. A pixel with the accumulated illumination above the threshold is called an *event*, which is the basic level of all GLM products. Adjacent events during the same 2 ms time window are clustered into a *group* (Mach et al., 2007). A group centroid is calculated in longitude/latitude coordinates. Group energy and group area are the energy and "footprint" of all the events associated with the group (Christian et al., 2000). Groups are frequently associated with a cloud pulse or a CG stroke reported by ground-based networks like the U.S. National Lightning Detection Network (NLDN) (Cummins & Murphy, 2009), but may be a combination of a few pulses within the 2 ms frame time. Groups that are within 330 ms and 16.5 km are evaluated to determine if they meet a Euclidian Distance criterion (Mach, 2020), and if so, they are clustered as a *flash*. Note that the GLM operational algorithm limits the number of events in groups and groups in flashes to nominally 101, and the flash duration to nominally 3 seconds (Mach, 2019; Mach, 2020), so GLM may split up large/long flashes. The GOES-16 GLM"Full Validation" study included in Koshak et al. (2018) also reported that the flash false alarm rate is currently higher than specified (as high as ~20% at times rather than 5%) but is expected to be greatly reduced after the glint filter was added on July 25th, 2019 (Rudlosky, S., personal communication). Finally, the GLM location is reported within a half a pixel near nadir, with somewhat larger variation towards limb (Rudlosky et al., 2019).

2.2. Lightning Imaging Sensor (LIS)

The TRMM-LIS which orbited with a 35° inclination is a precursor instrument of the GLM sensors. The full FOV of LIS was about 600 × 600 km after being boosted to a 402 km altitude in 2001, with approximate 90 seconds observation time for any single location on Earth during an overpass (Cecil et al., 2014). The total viewing time of LIS in the tropics was only about 0.1% (Cecil et al., 2015). Similar to GLM, LIS was also an

optical sensor, but with 128 × 128 pixels in the array and the pixel size of LIS was about 4 km by 4 km at nadir, which was four times higher spatial resolution than GLM. After 17 years on orbit, TRMM LIS ended its service in 2015. This was followed by placement of a second LIS instrument on the International Space Station, allowing simultaneous comparisons between LIS and GLM (Blakeslee et al., 2018). Given the rich, long-term TRMM LIS dataset and well-studied instrumentation and finer spatial resolution, LIS is the best reference instrument to help understand the nature of the GLM and its detection behaviors. In this study, TRMM-LIS data during the summertime of 2013 (June–July–August, JJA) are used to study the flash evolution of group-level products including group energy density and group area.

Noted that one of the group-level products in the archived TRMM LIS data (Blakeslee, 1998) is called "group radiance." In fact, this product is not exactly radiance, but spectral energy density (Koshak, 2010 in Appendix). These terms are considered interchangeable in this paper and both terms appear.

2.3. National Lightning Detection Network (NLDN)

The satellite-based optical sensors are limited in their ability to discriminate flash type for individual flashes, although statistical retrievals are possible (Koshak, 2010, 2011; Koshak & Solakiewicz, 2015). In order to separate CG flashes from intra-cloud (IC) flashes, this study uses additional measurements provided by the U.S. NLDN to help determine individual flash type.

The U.S. NLDN uses a combined time-of-arrival and direction-finding technology to locate lightning discharges (Cummins & Murphy, 2009). It provides real-time lightning data including time, location, peak current, as well as other data-quality and waveform information. The NLDN geo-locates lightning discharges with a median location accuracy of about 200 to 300 meters (Nag et al., 2014) with a time accuracy to the microsecond. The most recent system-wide upgrade of NLDN occurred during April–August in 2013, mainly to improve IC flashes detection (Murphy & Nag, 2015; Nag et al., 2014). A post-upgrade study shows that the IC flash detection efficiency increased to 50–60% (Murphy & Nag, 2015).

In this study, 3 months of NLDN data (2013 JJA) are used to determine the type for LIS flashes. In order to inter-compare LIS with other lightning locating systems (LLSs), certain temporal and spatial criteria for flashes are used, as described in Zhang et al. (2019). Any LIS flash that was space-and-time correlated with an NLDN-defined CG flash is defined as a LIS CG flash. Given the high (>90%) CG flash detection by the NLDN (Zhang et al., 2015; Zhu et al., 2016), all other LIS flashes are defined as LIS IC flashes, even though a great portion of them had no temporally and spatially matched NLDN reports. In addition, the NLDN CG data were also used to classify the LMA flashes (IC vs. CG) employed in this study to evaluate GLM performance in the vicinity of KSC in 2018–19.

2.4. Lightning Mapping Array (LMA)

The LMA at KSC locates the impulsive breakdown processes (sources) produced during a lightning flash by measuring the VHF electromagnetic radiation and employing time-of-arrival geolocation using 5 or more stations (Thomas et al., 2004). LMA's ability for mapping the fine structure of lightning with high accuracy has led it become the "ground-truth" dataset in this study. Note that the LMA was only used to inter-compare with GLM, but not for LIS, given its limited observation time due to the orbital nature of the satellite.

LMA sources were clustered into flashes using the approach described in section 2.5. The flashes were then used to estimate flash area, channel length and flash extent using a convex hull flash object described in Bruning and MacGorman (2013) and Bruning and Thomas (2015). The flash area is defined as the hull area, and flash extent is defined as major axis length of the convex hull. Flash length is defined as total path length of connected LMA sources from the two longest non-colinear axis limits back to flash origin, as shown in Figure 1. Note that this calculation of channel length is a direct calculation from the individual sources, rather than the fractal approach introduced by Bruning and Thomas (2015).

2.5. LMA Flash Matching and Flash Clustering

Care must be used when comparing lightning observations from different instruments, as they report different physical processes within a flash (Appendix C in Zhang, 2019). Satellite-based optical observations and ground-based VLF/LF observations are both well-suited to observe high currents in long channels, such as return strokes and processes associated with k-changes (Thomas et al., 2000; Ushio et al., 2002). On the other

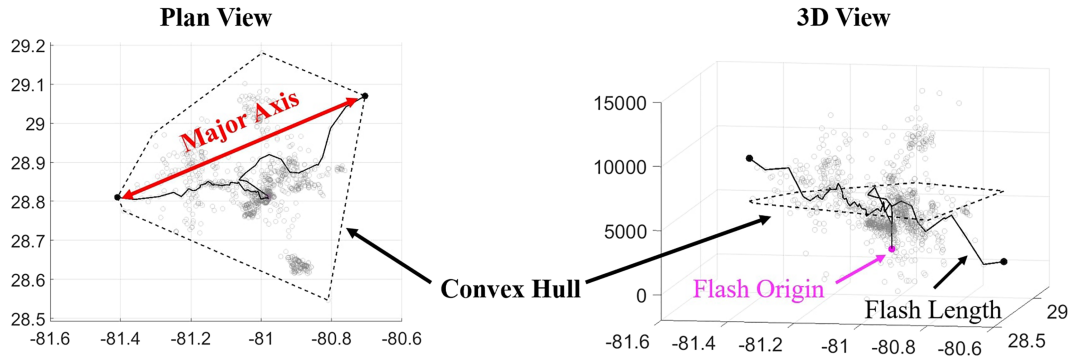

Figure 1. Plan view (left) and 3D view (right) of a flash and its convex hull. The flash area is shown as the 5-sided polygon. The flash extent is shown as the major axis in red. The flash length is shown as the black curve on the right between the flash origin and major flash endpoints.

hand, LMA systems, operating in the VHF frequency range, are well-suited to map-out breakdown processes during the establishment of new channels and branches. These differences will result in very different depictions of the spatial and temporal behavior of charge neutralization within/from an electrified cloud over time periods on the order of one second, which is commonly referred to as a lightning flash. The conceptual basis for the matching of flashes in this work is that LMA can be relied-upon to determine the start and duration of a flash, and to describe the set of possible 3-dimensional paths for higher-current processes seen by GLM, LIS, and NLDN. There is some possibility that a last high-current process might occur a few milliseconds after the last reported LMA source, such as a final return stroke in a CG flash. Given this background and motivation, the basic spatiotemporal domain for a flash in this work is defined by constructing "LMA flashes", and these flashes are then "matched" in space and time using the fundamental measurements provided by GLM (group time and centroid) and NLDN (CG stroke and cloud pulse times and locations). Note that the GLM and NLDN data were not clustered into flashes. This eliminates the complications due to differences in flash-grouping algorithms and process detection noted above. In this work, a "GLM match" to an LMA flash occurs if at least one group overlaps in-time (+/− 4 ms before/after the flash) with its centroid within 12.5 km (about 1.5 GLM pixels) of an LMA source in the flash. Similarly, an "NLDN match" to an LMA flash occurs if at least one cloud pulse or CG stroke report overlaps in the same time interval (+/− 4 ms), and is located within 4 km of any LMA source in the flash. We have confirmed that moderate variations in these matching parameter values had little impact on the estimated DE for GLM (not shown).

LMA flashes were assembled by grouping individual LMA sources using a 3-dimensional grouping algorithm first described by Lojou and Cummins (2005), similar to other flash algorithms (Fuchs et al., 2016; Murphy & Nag, 2015). Briefly, given an LMA source at some point-in-time (hereafter "new source"), the Euclidian distance to all earlier LMA sources within a prescribed time limit (0.3 s in this case) was computed. If one or more earlier sources were within a specified distance limit (5 km in this case), the new source was linked to the closest source. If either the temporal or spatial limits were exceeded, the new source became the first source in a new flash. To discourage inadvertent vertical connections due to simultaneous propagation of leaders, the distance in the z (height) direction) was scaled-up by a constant greater than 1.0 (in this case, 1.5), and an upper limit on instantaneous velocity was set to be 10^8 m/s. Finally, if flashes overlapped in space and time (using the same limits noted above), they were merged together, as was done by Fuchs et al. (2016). This resulted in both the clustering of sources into distinct spatio-temporal collections that we refer to as flashes, and information about the likely connections between sources in a flash that provides a basis for computing approximate channel lengths.

For this study, the KSC LMA was assumed to report and accurately characterize the spatial and temporal extent of all flashes. Although this is likely not the case, analyses of several LMA systems by Chmielewski and Bruning (2016) indicates that it is fair to assume at least 95% of all flashes within 100 km of the center of a properly maintained LMA system will be reported. Since the KSC LMA only had eight operational sensors during this study period, our estimates of flash counts, duration, and size should be viewed as lower bounds on the actual values.

Table 1
Summary of GLM Detection Efficiencies Relative to LMA in the 22 Storm Days at KSC Between 2018 and 2019

		GLM DE relative to LMA					
Date	LMA flash count	Overall	IC	CG	5–8 km	15–25 km	50–100 km
03/20/18	51,849	71.7	69.5	85.9	39.7	75	95.3
04/07/18	6,040	67	65.3	75.7	34.5	59.5	93.9
04/10/18	36,732	60.8	59.5	67.3	21.9	59.7	90.9
04/11/18	2,413	86.4	85.1	89.2	56	77.6	96.6
04/23/18	11,564	63.6	59.7	84	15.8	69	95.1
05/15/18	31,030	74.7	73.4	82.5	45.3	80.1	95.4
05/31/18	13,920	59.8	56.4	88	18.2	64.2	94.5
06/04/18	522	74.9	73.2	93.2	35.7	87.8	96.2
06/06/18	21,402	67.7	65.4	80	24.5	72.5	95.2
07/18/18	10,495	65.9	60.8	82.9	27.8	69.3	95
08/10/18	1,652	50.8	44.2	83.6	20.8	56.1	90.3
08/23/18	16,822	67	63.1	85	32.6	75.6	92.8
09/19/18	11,547	71.2	69.5	84.7	38.1	84.4	96.2
11/12/18	507	94.7	94.2	99.2	66.7	96.3	100
11/23/18	3,210	74.2	73.6	100	39.7	91.9	100
12/03/18	6,523	77	76	88.9	40.8	91.2	99.4
12/15/18	647	88.4	86.7	95.4	42.9	91.5	100
12/20/18	5,337	64.4	63.7	72.4	32.1	73.1	98.5
01/24/19	1,287	91.8	91.6	94.5	62.2	91.2	100
02/12/19	4,919	84.3	83.8	91.2	52	93	99.8
02/13/19	2,261	98.3	98.3	98.9	92.3	98.8	100
02/27/19	527	85.2	83.3	100	72.4	80.8	100
Total	241,206	73.8	71.8	86.5	40.4	77.8	96.3

Note. Nighttime observations are highlighted in gray. The last three columns are for different channel lengths.

3. Results

3.1. GLM Detection Efficiencies

Many types of storms (including isolated cells, mesoscale systems, and squall lines) were analyzed in the KSC area for 22 days between March 2018 and February 2019. In total, 241,206 LMA flashes (those having a minimum of 10 LMA sources) were evaluated. In all cases, the GLM flash detection efficiency increased with increasing LMA flash duration, increasing flash area, longer channel length, and longer flash extent. Table 1 summarizes the daily GLM flash detection efficiencies relative to LMA for different channel lengths. The daily GLM flash detection efficiency ranged from 51% to 98% with an average value of 73.8%, which meets the full-disk design specification. The average daily nighttime (total darkness) detection efficiency was 87.8%.

Table 1 clearly indicates that for each of the 22 days, the GLM flash detection efficiency increased with increasing channel length (last three columns in Table 1). For flashes with short channel length (5–8 km), the GLM flash detection efficiencies ranged from less than 20% to a little over 90% but was typically between 30–50% with an overall average of 40.4%. On the other hand, the detection efficiencies for flashes with extremely long channel length (50–100 km) generally exceeded 95%. The overall average flash detection efficiency was 77.8% for flashes that extended 15–25 km horizontally.

GLM had its best performance for the winter-time storms between November 2018 and February 2019. All nine of these cases were associated with wide-area disturbances due to various kinds of synoptic-scale forcing, but they exhibited varying depths and densities of embedded convection. Four of these cases occurred at night (highlighted rows in Table 1). The day:night difference is illustrated by the February 13, 2019 case (overall 98.3% detection), which is a continuation of the daytime case on February 12, 2019 (overall 84.3% detection). The three daytime winter cases with overall detection efficiency above 80% involved only shallow (low-topped) storm cells with low flash-rates, whereas the November 23, 2019 nighttime case (overall 74.2% detection) included many high flash-rate cells with expected size of hail between 0.5 and 2 inches based on the NEXRAD MESH product. We note that for most of the cases with overall detection efficiency above 80%,

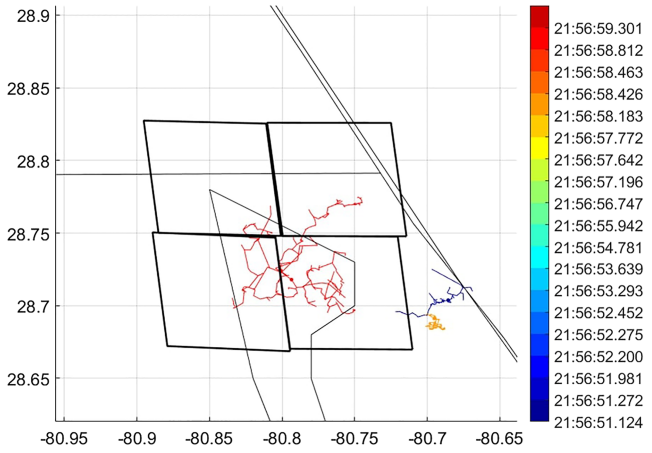

Figure 2. Plan view of three LMA flashes at Kennedy Space Center during 21:56:50 to 21:57:00 on march 20th, 2018, colored by start-of-flash time. The black squares outline the GLM pixels associated with the large (red) flash. The other two flashes were not reported by GLM (see paper for details).

the detection of small flashes (5–8 km) was also quite good. A detailed assessment of variations of GLM performance with season and storm-evolution is outside the scope of this work but is a much-needed area or research. Given these seasonal and case-day variations, along with known variations in GLM detection thresholds by region (Cummins, 2019; Said, 2019; Yoshida, 2019), we expect somewhat different GLM performance in different regions and seasons.

Figure 2 provides an illustrative example by depicting a plan view of three flashes detected by the LMA during a 10-second period (21:56:50–21:57:00) on March 20th, 2018 at KSC. The GLM pixels (shown as black polygons) fully-cover and were time-coincident with the larger flash in red, which was an IC flash with source heights up to 9.8 km. The two other smaller flashes were not reported by GLM. The first flash (blue) was a small IC flash with an LMA duration of 0.3 s and a maximum source height of 4.4 km. The second flash (orange) in this example had an LMA duration of 0.106 s, a maximum source height of 5.6 km, and was associated with a single-stroke negative CG flash reported by the NLDN with an estimated peak current of −10.8 kA. One broadly accepted reason for lower-detection of some flashes is that the cloud-top illuminations from flashes deep within the cloud are scattered by the cloud body (Boccippio et al., 2001; Light et al., 2001; Thomas et al., 2000). As Thomas et al. (2000) pointed out, optical emissions that are associated with discharges in the middle or lower part of the storms (i.e. downward leaders and associated CG strokes) are less likely to be detected by satellite sensors, assuming equivalent light sources.

Results from a representative mesoscale convective system during a two-hour period (18:00–19:59 on March 20th, 2018) are shown in Figure 3. The GLM flash detection efficiency relative to the LMA during this period was 67.0% (11,896/17,758) with IC and CG flash detection efficiencies being 63.6% (9,318/14,652) and 83% (2,578/3,106), respectively. Overall, GLM reported about 20% of the flashes with duration less than 100 ms (about 50 GLM frames) and over 60% when the flash duration was longer than 300 ms (about 150 GLM frames). When the flash duration was over 500 ms (about 250 GLM frames), GLM reported more than 80% of the flashes. Similarly, when the flash channel length was less than 5 km (shorter than one GLM pixel and about one LIS pixel), the GLM flash detection efficiency was less than 20%, whereas when the channel length was over 25 km (3–4 GLM pixels and 6–7 LIS pixels), the flash detection efficiency was over 85%. This is also consistent with our general sense that the longer the flash duration, the longer the channel propagates and develops in space, and hence, result in larger flash area and larger flash extent.

Interestingly, CG flash detection efficiency during this study period is greater than that of IC flashes, which is inconsistent with earlier expectations (Thomason & Krider, 1982) and LIS observations (Franklin, 2013; Thomas et al., 2000). For all the 22 days, GLM showed a higher detection efficiency for CGs than ICs (Table 1). The average daily IC and CG flash detection efficiencies were 71.8% and 86.5%, respectively. Also, the detection efficiencies are more variable for ICs than for CGs. Our findings are consistent with Yoshida's results (Yoshida, 2019) who studied the GLM IC/CG DE within the entire FOV, and hence, provide further evidence that the GLM preferentially detects CG flashes (versus IC). Our preliminary examination of individual flashes indicates that the GLM tended to detect illuminations associated with strokes in CG flashes, especially first strokes. These strokes often produced a relatively brighter and larger illumination at the cloud-top than other lightning processes, even though they typically occur in the lower portion of the clouds. Some very short CG flashes reported by LIS were found to produce very bright illuminations (see discussion in section 3.2). In addition, more than 50% of the CG flashes in this study included at least three sources above 10 km altitude, which was only 1 km lower than the associated value for IC flashes. This suggests that a great portion of the NLDN-defined CG flashes from the studied area during our study period were hybrid flashes that include significant upper-level in-cloud discharges. Further study on hybrid flashes detection by the satellite is needed to fully understand these observational results.

In our earlier, preliminary work using only 67 flashes (Zhang et al., 2017), GLM was reported to detect initial breakdown process (processes in the first 50 ms from the first LMA source, which is considered as the start of

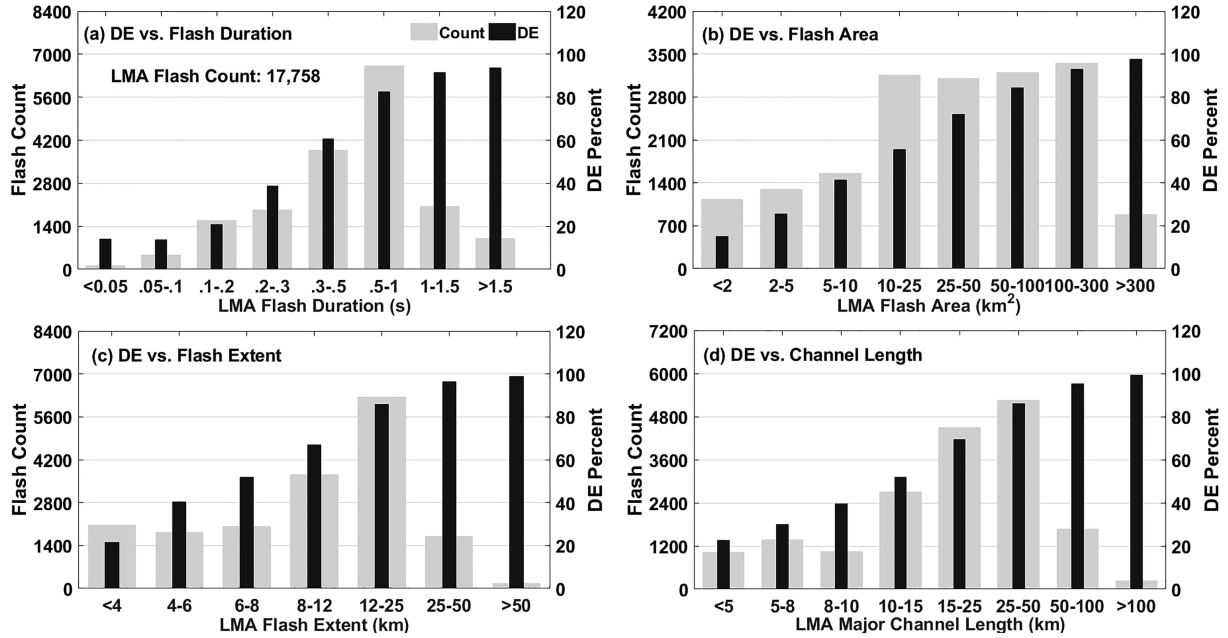

Figure 3. GLM flash detection efficiency (DE, black bars) during 18:00–19:59 on march 20th, 2018 with respect to flash duration (top left), flash area (top right), flash extent (bottom left) and channel length (bottom right). The number of flashes are shown as wide gray bars.

the flash) in half of the flashes with channel lengths greater than 50 km. Figure 4 shows results for a much larger dataset (the storm case shown in Figure 3). Initial breakdown was reported in 20.4% of the flashes with channel lengths greater than 30 km, with lower values for smaller flashes. The "detection latencies" range from a few tens of milliseconds, up to a few hundred milliseconds, even for flashes with horizontally-extensive channels. The 50th percentile latency is about 150 ms for flashes over a wide range of channel lengths (see Figure 4). In other words, about half of the flashes detected by GLM started about 150 ms after the LMA first source. These behaviors may have a similar origin as the behavior of not detecting small and short flashes. This may be because the initial high-current processes must be constrained to smaller spatial areas than later processes in larger flashes, as a result of the finite propagation speeds of leaders associated with initial breakdown (about one kilometer in 2–10 ms).

3.2. Flash Evolution of Group Parameters

Given the impact of flash duration and size on GLM detection, the possibility exists for optical source brightness and size to vary as a function of the time-evolution of a flash. This was explored by computing group

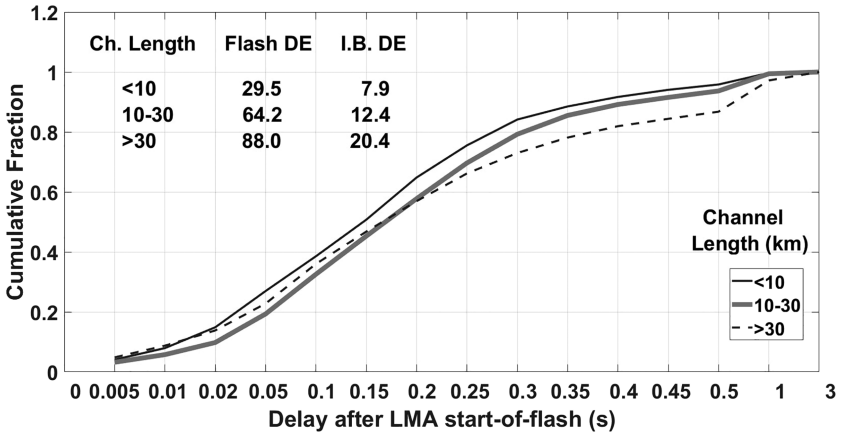

Figure 4. Cumulative fraction of the GLM flash latency after the LMA-reported start-of-flashes for various ranges of channel lengths. The table indicates the flash DE and DE for initial breakdown (I.B. DE) for the same ranges of channel lengths.

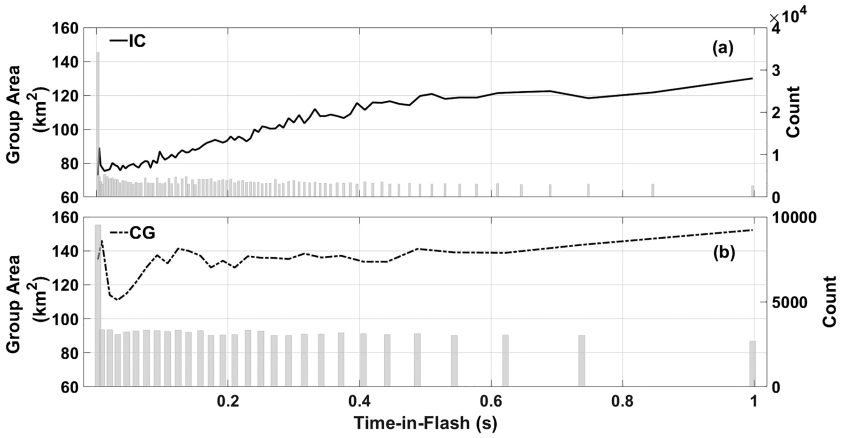

Figure 5. LIS flash time evolution of mean group area in intra-cloud flashes (solid, top) and cloud-to-ground (dash-dotted, bottom) within the NLDN coverage during 2013 JJA. The sampling intervals are longer as time-in-flash increases, due to the smaller number of longer-duration flashes. The gray bars are the count (shown on the right) in the bins. Note that the data were cut off at one second in the figures due to the small number of flashes longer than one second.

parameter statistics (mean count, and standard deviation) as a function of time after the start of each LIS flash. LIS data were used for this analysis because of its smaller pixel size and its ability to detect smaller, lower-energy sources than GLM (see Appendix A). In general, the time-in-flash evolution of LIS group parameter mean values show similar patterns in both group area and group energy density for both IC and CG flashes, as shown in Figures 5 and 6. It was found that both LIS group area and group optical energy density in IC flashes reached an initial peak value in the first few milliseconds. These early times in flash formation correspond to preliminary breakdown in a flash which is observed to be bright over a modest-sized area. Following the early peak, the two group parameters decrease to minimum values after about 10–30 milliseconds into the flash. Both parameters then increase gradually over the next 100–150 milliseconds when they return back to the initial value at the beginning of the flash, and then continue to increase. The early peaks of both group parameters for IC flashes are probably associated with the optical emissions from the initial breakdown processes that are relatively high in the cloud and are produced by currents in vertically extensive channels between the mid-level and upper charge regions. Although the mean group area is relatively large within the first 4 ms (about 80–90 km^2, or about 5 LIS pixels), our modeling analysis in Appendix B indicates that about half of the optical sources that illuminate less than 5 LIS pixels are likely to be smaller than or equal to the size of a single LIS pixel (about ¼ of a GLM pixel).

Interestingly, there is a distinct difference in the optical characteristics between IC and CG flashes over the U. S., differing from the early space-based observations reported by Goodman et al. (1988). Overall, both group area and group energy density for CG flashes have larger values than for IC flashes. For instance, the initial

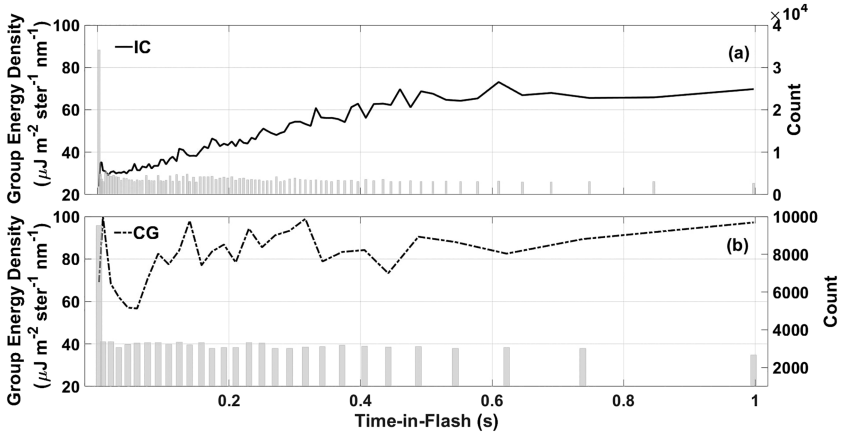

Figure 6. Same as Figure 5, but for group energy density.

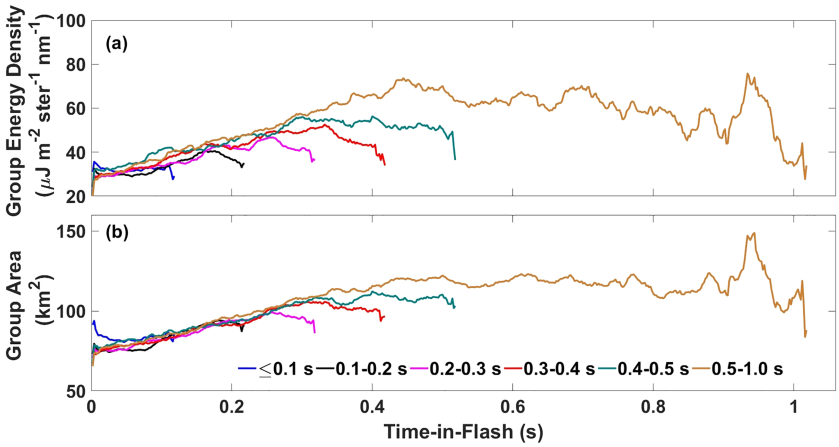

Figure 7. Time evolution of mean group energy density a and group area b for different durations of LIS IC flashes.

peak values for CG flashes are 1.5–2 times larger (see Figures 5 and 6). These large values at the very beginning of the flashes are frequently associated with the first return strokes, as the very first optical signals that LIS observed in a large portion of CG flashes were associated with first return strokes, and the optical signals are usually larger due to the high current flowing in the long return-stroke channels. Unlike IC flashes, there is no gradually rising pattern for group radiance or area throughout the later part of the flash in CG flashes.

The time-in-flash evolution of LIS IC group parameters for various flash durations (Figure 7) shows a similar pattern as the overall IC flash pattern, with a local peak at the very beginning, followed by a rapid fall-off and a gradual rise. The only difference is that there is a rapid decrease in both group area and group energy density at the end of the flashes for all flash durations. This decrease is more obvious in the group energy density and may be related to a reduced likelihood of high-current processes in the horizontal channels near the end of a flash. Note that there are about 15–20% larger values near the beginning of the very short flashes (less than 100 ms) in both group energy density and group area. These large values occurred for very short flashes (usually less than 5 ms, single- or two-group flashes) with a very bright group in the first or the second frame. Further investigation of these very bright but short flashes is needed.

4. Discussion of GLM Detection Behavior

Here we strive to explain the dependence of GLM detection on the flash parameters presented in section 3.1 using (1) the LIS time-in-flash observations reported in section 3.2, (2) further observations in this section, and (3) results provided in Appendices A and B. We begin with a formulation of detection that encompasses both GLM and LIS, followed by an effort to characterize the size and energy of the underlying cloud-top optical sources that produce LIS and GLM groups. The final analysis combines all these to estimate the variations in GLM detection as a function of time-in-flash.

In order to relate LIS group parameters to GLM detection, a common parameter space for both instruments is needed that does not depend on differences in the satellite orbits or the optical properties of the instruments. Cloud-top optical energy (in Joules) has this property, and it can be estimated for both instruments using publicly available GLM and LIS group-level products. The formulations provided in Appendix A result in the following expressions for group-level cloud-top energy in Joules:

$$\text{LIS Group Cloudtop Energy} = \frac{2.83\text{A}\widehat{\xi}}{\text{n}} \tag{1}$$

$$\text{GLM Group Cloudtop Energy} = \frac{6.61\text{A}\widehat{\text{q}}}{\text{n}} \tag{2}$$

where n is the number of events (pixels) in the group and A is the group area in km^2. The standard LIS group radiance ($\widehat{\xi}$) is assumed to be expressed in units of μJ m^{-2} ster^{-1} nm^{-1}, and the standard GLM intercepted energy ($\widehat{q}$) is assumed to be expressed in units of femtojoules.

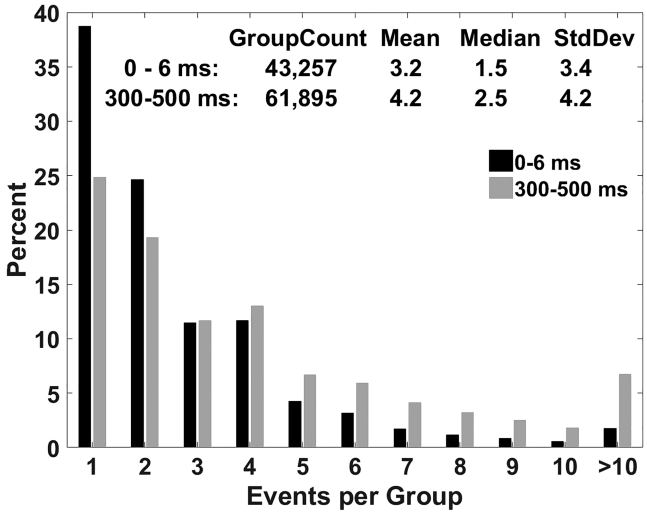

Figure 8. Histograms of events per group for 0–6 ms (black) and 300–500 ms (gray) for LIS IC flashes.

Appendix A also discusses the fact that LIS and GLM detection behavior is dependent on the specific nature of the cloud-to optical source. For sources smaller than a LIS pixel, the minimum-detectable cloud-top energy is about 2.58-times lower for LIS than for GLM. However, if the optical energy is spread uniformly over the much-larger area of a GLM pixel (typically about 4 times larger than a LIS pixel), then a just-detectable cloud-top source for GLM would not be reported by LIS because the total energy within any one LIS pixel would be below its detection threshold.

Cloud-top optical source size interacts with pixel size in another way, impacting detection capabilities of both instruments. If the source covers a significant fraction of a pixel, then so-called "pixel splitting" becomes an issue (see Appendix B) for both sensors, but more-so for LIS due to its smaller pixels (more opportunities for splitting). Pixel splitting can result in an over-estimate of cloud-top source area for sources well-above the detection threshold, or a loss of detection for sources close to the detection threshold. These complications related to group area have led us to look more-closely at the size of cloud-top optical sources reported by LIS.

The histograms of events-per-group in Figure 8 (for LIS IC flashes) show that small-size groups (fewer events-per-group) occur much more frequently than large-size groups. This is particularly true for groups that occur early in the flash during initial breakdown (0–6 ms dataset), and less-so for groups that occur later in longer-duration flashes (300–500 ms dataset). Overall, the most-common number of events in a group was one, indicating that many sources are either smaller than or about equal to the size of a single LIS pixel (~4 km × 4 km), as discussed in Appendix B. Overall, the percentage (frequency of occurrence) decreases with increasing events-per-group. An interesting exception is that the category of three events per LIS group occurs less frequently than four. Our hypothesis for these behaviors is that a large fraction of the light sources at the cloud top detected by LIS were much smaller than a LIS pixel, making it difficult to uniquely illuminate three pixels. Modeling results provided in Appendix B show that small light sources are required in order to produce events-per-group distributions that are consistent with observed ones shown in Figure 8. Our interpretation of these findings are that (1) a large fraction of the cloud-top optical sources are smaller than a LIS pixel, and (2) the group area for sources associated with 2–4 events-per-group is a significant over-estimate of the actual area of the bright portion of cloud-top sources as a result of "pixel splitting."

Moving on to the time-evolution of optical source parameters throughout a flash, our findings shown in Figure 5 indicate that the mean group area increases over the lifecycle of IC flashes, after the first 10 ms. Comparison of the histograms between 0–6 ms (beginning) and 300–500 ms (later) in the flash (see Figure 8) also shows a higher fraction of events-per-group at later times in the flash than at the beginning of the flash. At the later times, 25% of the groups had a single event, compared to 39% at the beginning of the flash (~35% fewer), and groups having more than 4 pixels occurred about twice as often. The mean values for the beginning and later time are 3.2 and 4.2 events per group, respectively. In other words, the cloud-top light sources occupy (on average) one additional pixel in the later time in the flash than at the beginning. According to the modeling results in Appendix B, the mean value of 3.2 (median of 1.5) events-per-group, coupled with a high percentage of single events-per-group cases, is likely to be produced by light sources varying in size between less-than-one and close-to-one LIS pixel. Later in long-duration flashes, with a mean value of 4.2 events-per-group and a median of 2.3, there should be a larger contribution from cloud-top sources that are much larger than a LIS pixel.

Based on the threshold analyses in Appendix A and earlier discussion in this section, GLM is more likely to detect larger cloud-top optical sources (larger than 4 LIS pixels), which preferentially occur at later times in the flash. This is consistent with our GLM latency statistics shown in Figure 4. This figure also indicates that although only about 50% of the earlier part of long-duration flashes (first 150–200 ms) was reported by GLM, GLM reported about 80% of the later part (> 300 ms) of the flashes. This behavior is also consistent with the LIS time evolution plots shown in section 3.2, showing that the IC flashes have, on average, a lower energy density (Figure 6) and are smaller in size (Figure 5) during the first 150 ms of the flash.

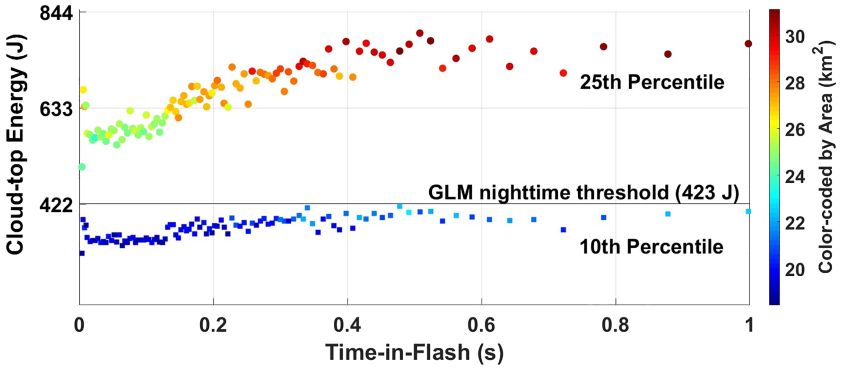

Figure 9. Time evolution of group cloud-top energy (joules) in the 10th and 25th percentiles, color-coded by the group area for LIS IC flashes. The black line shows the GLM nighttime threshold, which is 423 J.

To get a lower-bound estimate of how frequently lightning optical source amplitudes fall below the GLM detection threshold, we evaluate the cloud-top optical energy received by LIS that could be reported by GLM (see Figure 9). In this figure, the data shown in Figures 5a and 6a, along with the associated information about the number of pixels in each LIS group, are used to produce cloud-top energy based on equation (1). These data are then aggregated into ranges for time-in-flash, resulting in collections of hundreds of values for each range. Scatter plots for the 10th and 25th percentiles of these collections are shown in Figure 9, color-coded by group area. Note that the group areas (means for each collection and percentile) for all these data are between 18 and 32 km^2 (about 1–2 events-per-group), strongly indicating optical sources smaller than a LIS pixel based on the analysis in Appendix B. The values in Figure 9 can be directly compared to the nighttime thresholds of cloud-top energy for GLM (423 J – see Appendix A), and this value is used in the figure as one of the horizontal grid lines. It is found that the groups in the lowest 10th percentile (lower curve) have energy amplitudes that remain less than the GLM nighttime threshold (423 J) for the duration of the flash. Similarly, the lowest 25th percentile is less than twice the GLM nighttime threshold (846 J). In other words, the GLM nighttime threshold indicates that GLM would not detect 10% of LIS groups. In addition, the intermediate value of 634 J, thought to be a typical daytime threshold for GLM in Florida, would eliminate 25% of the weakest LIS groups out to a latency (delay after start of flash) of about first 150–200 ms. These findings clearly show that small and dim cloud-top optical sources tend to occur at the beginning of the flashes.

These findings provide a clear basis for the GLM detection findings in section 3.1. LIS could be used to explore and explain these behaviors because (1) most near-threshold sources were much smaller than a GLM pixel (and somewhat smaller than a LIS pixel), (2) the cloud-top energy detection threshold is lower for LIS than for GLM for these small optical sources, and (3) smaller cloud-top optical sources tend to occur at the beginning of the flashes.

Although a simultaneous comparison between TRMM LIS and GLM is not possible, the second LIS (a spare instrument for TRMM LIS) on the International Space Station (ISS) will have simultaneous observations with GLMs. A logical next step is to use the ISS LIS data to further study the GLM detection behaviors using the time-in-flash method shown here.

5. Conclusions and Closing Comments

In general, the GLM flash detection efficiency increases with channel length and flash duration. These results are based on a full year of GLM observations over KSC, with no restriction on flash rate, storm cycle, storm type, or cloud scattering/absorption. Therefore, it is likely that the channel length and flash duration are two of the key factors impacting satellite-based optical detection, particularly for the relatively large pixel size employed by GLM. Given the seasonal and case-day variations, along with known variations in GLM detection thresholds by region, we expect different GLM performance in different regions and seasons.

Unlike what was expected for an optical sensor and what was observed by TRMM LIS, the GLM had an overall higher detection efficiency for CGs than ICs. A possible reason for this behavior is that optical sources in

the CG flashes have brighter and/or larger groups (see Figures 5-6), which are easier for GLM to detect. This supports other preliminary findings and suggests that further investigation is needed.

The findings related to the time-evolution of cloud-top optical sources based on 3 months LIS observations seem to explain the poor detection of short-duration IC flashes (less than 100–150 ms) seen in our study of GLM performance at KSC. If GLM does not detect optical sources in the first few milliseconds of a flash associated with the preliminary breakdown, it may not detect any optical emission for more than 100 ms. This is because a flash takes time to develope into a spatially expansive area and produce larger and brighter optical sources (see Figures 5-9). Short-duration IC flashes do not last long enough for the channels to develop and grow sufficiently long to produce bright and large sources for GLM to detect. Additionally, since short duration flashes frequently occur during severe storms (Bruning et al., 2010), the fraction of flashes detected by GLM for these storms can be quite low. These findings are consistent with recent studies carried out during GLM validation (Hilburn et al., 2019; Thomas et al., 2019), but here we focus on optical source properties rather than cloud optical depth.

In closing, we note that there is a potential for performance improvement in the future. The existing (operational) configuration enforces conservative space:time coherency among adjacent pixels that may be too strict. The growing set of observations and validation studies are leading to new insights about the behavior of lightning and non-lightning sources. Given the large number of below-threshold cloud-top sources produced by lightning, even modest algorithmic improvements could lead to meaningful improvements in the detection of short duration and/or physically small flashes by GLM.

Appendix A: Cloud-Top Energy and Instrument Detection Thresholds

GLM and LIS orbit at different altitudes with different sensitivities, and also provide different group-level data products (energy and spectral energy density, respectively, incident at the pixel array). In order to inter-compare group-level data and detection thresholds for these instruments, we have elected to convert LIS spectral energy density (ξ_λ, in μJ m^{-2} ster^{-1} nm^{-1}) and GLM energy intercepted by the satellite detector (denoted q, in units of J) to cloud-top energy (E, in J). This parameter depends directly on the characteristics of the optical source within the cloud, but not on the instrument's optical characteristics. This is also an excellent parameter for characterizing threshold since, under reasonable conditions, it is the cloud-top energy within the field of view of a pixel that determines if an optical source will be reported by that pixel. With this formulation, it becomes clear that the input to a pixel can be produced by a very small but "bright" (high energy density) source, or by a lower energy density source that fills more of the pixel area (footprint). Complications due to source energy being split among multiple pixels, such as when it is centered on the boundary between multiple pixels (so-called "pixel splitting") is explored in Appendix B. The cloud-top energy formulations are provided below. For brevity and clarity, we now drop the lambda subscript on spectral energy density. Also note that the LIS spectral energy density is loosely referred to as the LIS "radiance" data product in the Level 2 data distribution (see the Appendix of Koshak, 2010 for additional details on terminology and radiometric definitions).

The LIS event radiance values for a group (i.e., the set of solid-angle-averaged spectral energy densities $\overline{\xi}_j$ comprising an optical group within a 2 ms instrument frame) can be converted to cloud-top energy (E) assuming that the cloud-top light is emitted isotropically (Koshak, 2017 – see equation (2)):

$$\mathrm{E} = \pi \Delta\lambda \sum_{\mathrm{j}=1}^{\mathrm{n}} \overline{\xi}_{\mathrm{j}} \mathrm{a}_{\mathrm{j}} \tag{A1}$$

where we have multiplied Koshak's equation (2) by $\Delta\lambda$ in order to obtain the energy within the optical bandwidth, and have limited it to a single frame (group) time. The quantity a_j denotes the footprint of the j^{th} pixel within the group. A very close approximation to A1 can be obtained from the group area and $\overline{\xi}_j$ values as follows. The LIS group radiance product (denoted here as $\widehat{\xi}$) is defined as the sum of the individual pixel event radiance data product values:

$$\widehat{\xi} = \sum_{j=1}^{n} \overline{\xi}_j. \tag{A2}$$

Since all the pixels within a group are adjacent to each other, it is reasonable to assume that their areas are nearly identical, specifically

$$\bar{a} = \frac{1}{n}\sum_{j=1}^{n} a_j = A/n \tag{A3}$$

where $\bar{a}$ is defined as the average area for the pixels in the group, n is the number of pixels in the group, and A is the group area. Substituting A2 and A3 into A1 yields

$$E = \frac{\pi \Delta\lambda \hat{\xi} A}{n}. \tag{A4}$$

Given the specified bandwidth ($\Delta\lambda$) of LIS as 0.909 nm, the rest of the values in equation A4 are available as standard LIS group product variables. Assuming that the group area is expressed in units of km^2 and that the group radiance is expressed in units of $\mu J\ m^{-2}\ ster^{-1}\ nm^{-1}$, equation A4 simplifies to

$$E = \frac{2.86 \hat{\xi} A}{n} \tag{A5}$$

The GLM energy intercepted by the satellite detector (q) values for a group can also be converted to cloud-top energy using the same isotropic assumption. Equation (5) in (Koshak, 2017) provides a way to transform the GLM group energy into the same radiance product as LIS:

$$\bar{\xi}_j = \frac{q_j}{\frac{\pi D^2}{4} \Delta w_j \Delta\lambda} \tag{A6}$$

Where $\bar{\xi}_j$ is the spectral energy density (radiance product) for pixel j during a single frame time, D is the sensor entrance pupil diameter in meters, Δw_j is the pixel solid angle, and $\Delta\lambda$ is the sensor bandwidth. Equation A6 can be substituted into equation A1 to obtain cloud-top group energy:

$$E = \pi \Delta\lambda \sum_{j=1}^{n} \left[\frac{q_j a_j}{\frac{\pi D^2}{4} \Delta w_j \Delta\lambda} \right] = \sum_{j=1}^{n} \frac{4 q_j a_j}{D^2 \Delta w_j}. \tag{A7}$$

The same "similar pixel area" assumption used for equation A3 can be used to make a_j independent of j, by employing its average value. Similarly, given the pixel solid angles within a group will also be nearly identical, Δw_j can be represented by its average as a constant ($\overline{\Delta w}$). Finally, the fact that the GLM group energy product (referred to here as $\hat{q}$) is defined as the total energy summed over all the pixels in the group, the cloud-top group energy in equation A7 can be expressed as

$$E = \frac{4 A \hat{q}}{n \overline{\Delta w} D^2} \tag{A8}$$

where n is the number of pixels in the group and A is the group area.

Equation A8 can be further simplified if the pixels are located towards the center of the field-of-view, where the solid angle is essentially constant (5×10^{-8} ster). The GLM entrance aperture is 0.11 m, and the bandwidth is 1 nm. Therefore equation A8 can be expressed as

$$E = \frac{6.61 A \hat{q}}{n}\ , \tag{A9}$$

where the group area A is expressed in km^2 and the group energy intercepted by the satellite detector ($\hat{q}$) is expressed in fJ (femtojoules).

Equation A5 is used in this report to convert long-term LIS group radiance values to cloud-top energy. In addition, the approximate nighttime minimum detection threshold for LIS can be derived using

equations A4 or A5 along with knowledge of the minimum pixel radiance threshold that was recently characterized by Zhang et al. (2019). These authors found minimum detected radiance (spectral energy density) values of 2.9 to 3.6 μJ/m^2/ster/nm, depending on the quadrant in the LIS pixel array. These low values were obtained at small off-boresight angles (near the center of the pixel array) and are consistent with nighttime minimum values reported by Boccippio et al. (2002). They also showed that the minimum threshold) increased to 5–6 μJ/m^{-2}/ster/nm during bright daylight – about double the nighttime values. Assuming a minimum value of 3.6 μJ/m^2/ster/nm, and a typical pixel size of 4 km × 4 km, the estimated minimum single-pixel ($n = 1$) cloud-top energy for a LIS pixel is

$$E = \frac{\pi \Delta \lambda \widehat{\xi} A}{n} = \pi(0.909)(3.6)(16) = 164 \text{ J}. \tag{A10}$$

It is important to note that if the light from such a threshold-level source is distributed over more than one LIS pixel, that it will not be reported by LIS. This issue is addressed further in Appendix B.

In a similar manner, the minimum cloud-top energy for GLM can be obtained using equation A9 and knowledge of the minimum value for the intercepted energy during nighttime conditions. This value varies somewhat throughout the GLM field-of-view, but within its inner 1/3, the most-common minimum value is 1.0 fJ (S. Edgington, personal communication, 2019). Given this and a typical pixel size of 8 km x 8 km in this region, the estimated minimum single-pixel cloud-top energy for a GLM pixel ($n = 1$) is

$$E = \frac{6.61 A \, \hat{q}}{n} = 6.61(64)(1.0) = 423 \text{ J}. \tag{A11}$$

The detection threshold for GLM in this inner field-of-view varies somewhat with time of day and other factors impacting the background illumination, but the values are typically in the range of 1.5–2 times this value.

Therefore, the minimum detectable cloud-top energy for a GLM pixel is (423/164) = 2.58 times higher than for a LIS pixel. The actual ratio will depend on the time-evolution of time-dependent and background-adjusted thresholds for the two sensors, as well as the viewing (off-boresight) angle and cloud-viewing geometry (fore-shortening angle), and requires a more-detailed analysis.

However, if the optical energy is spread uniformly over the area of a GLM pixel (typically about 4 times larger than a LIS pixel), then a near-threshold cloud-top source for GLM would not be reported by LIS. In other words, the GLM reports lower energy density of large cloud-top sources than LIS. Given the LIS minimum pixel spectral energy density of 3.6 μJ/m^2/ster/nm, the minimum cloud-top energy density of a single LIS pixel is:

$$E_{dens} \cong \frac{2.86 \xi}{n} = 2.86(3.6) = 10.25 \text{ J} \cdot km^{-2} \tag{A12}$$

And the minimum cloud-top energy density of a single GLM pixel is:

$$E = \frac{6.61 \widehat{q}}{n} = 6.61(1.0) = 6.6 \text{ J} \cdot km^{-2} \tag{A13}$$

Therefore, the GLM energy density threshold is 6.6/10.25 = 0.64 times smaller than LIS, which means that GLM reports lower energy density of large cloud-top sources (larger than 3–4 LIS pixels).

Appendix B: Pixel Splitting and Light Source Modeling

The similarity between the two GLM detection behaviors (dependence on flash duration and flash size) discussed in the body of this paper is likely because a short duration flash is also spatially small, so a large number of the light sources at the cloud top (determined by lengths of channels with high currents) must be relatively small. This appendix focuses on estimating the actual cloud-top source size by comparing model-based results with measured TRMM-LIS group information, which has a higher spatial resolution than GLM.

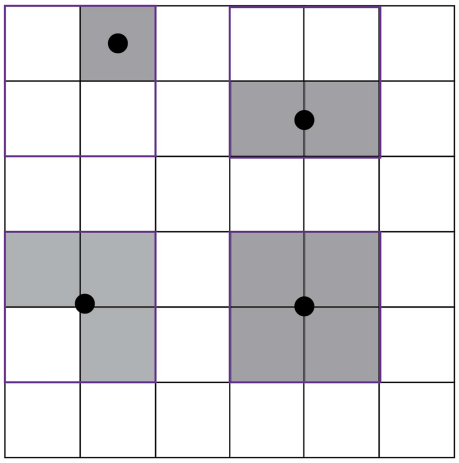

Figure B1. Illustration of 4 small simulated light sources and their relevant lit-up LIS pixels. The black boxes are LIS pixels, and thick outlined boxes are the associated GLM pixels. Black dots are light sources and gray shades are the pixels that are lit up by the light sources.

Before describing the model, we introduce the concept and nature of "pixel splitting" by satellite optical sensors, in the context of small optical sources. Shown in Figure B1, a small light source relative to LIS in the middle of a LIS pixel will "light up" only one LIS pixel, if it is bright enough (upper-left case). A small light source in between two adjacent pixels may light up both pixels (upper-right case). A small but bright source in the middle of four adjacent pixels may light up four pixels (lower-right case). Three pixels will only be lit up when a small light source with just the right brightness is in a very specific position relative to adjacent pixels (lower-left case), so it is less likely to occur. This simple illustration supports fewer cases of three events in a group. Since a LIS pixel is about four times smaller than a GLM pixel, such small light sources will be even smaller relative to GLM pixels. In the extreme case, a sub-kilometer cloud-top light source with very high energy could result in a 64 km^2 LIS group and a 256 km^2 GLM group.

Given this pixel-splitting behavior, the actual size of small optical sources cannot be assumed to be the measured group areas or pixel counts. Instead, a statistical model can be used to relate various (given) sizes of light sources to the number of events in a group, which can then be compared to the measured TRMM-LIS data. The model was constructed as follows. First, we created an array the size of 10 × 10 "nominal" LIS pixels. To be consistent with the real LIS observations, each pixel was set to be a 4 km by 4 km square. In each of these pixels, 400 small boxes with a 0.2 km sides were created. Second, light sources with three different sizes (small, medium, and large) were produced. The brightness of the light sources were normally distributed in all directions, with a total energy that varied with the size of the optical source in order to approximate median values reported by LIS. For this analysis, the exact source energy values are not critical. They were selected in-combination with the thresholds in order to nicely illustrate the interaction between pixel size and threshold with the phenomenon of pixel splitting. The small-size light source had most of its energy (1000 J) in an area of about ¼ of a LIS pixel, with a standard deviation of 3

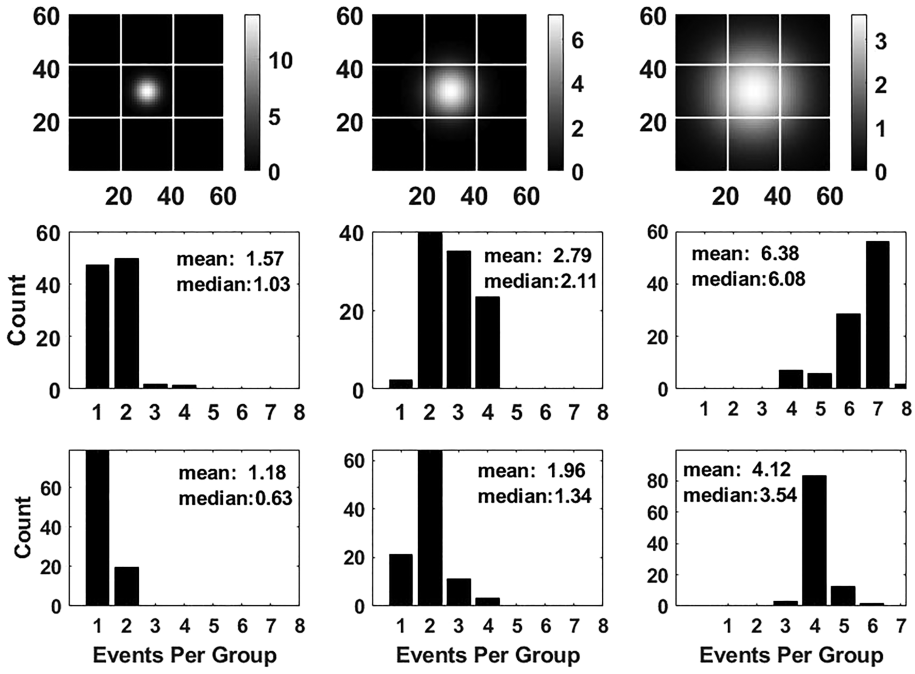

Figure B2. Results from the light source modeling using a 10x10 LIS pixel array. The top panels are the modeled three sizes of light sources in the central 9 LIS pixels. The middle (bottom) panels are the LIS population histogram of the number of events exceeded a low (high) threshold of 158 (316) J.

small boxes. The medium-size source was the size of about one pixel, with a standard deviation of 7 small boxes, and the large-size was larger than one pixel with a standard deviation of 13 small boxes, as shown in Figure B2 (top row). Third, two detection thresholds were selected – a value approximating the energy minimum threshold for LIS (158 J) which is representative for nighttime observations, and twice that value (316 J), which is representative for daytime observations. Fourth, the light sources were then centered on each of the 40,000 0.2 km by 0.2 km box positions and the energy in each pixel was computed. The number of pixels that exceeded the threshold were recorded. Lastly, the population histograms for the six conditions (3 sizes and 2 thresholds) were created using the inner 8x8 LIS pixel array, in order to avoid edge effects. These histograms are shown in Figure B2 (middle and bottom rows) for the low and high thresholds respectively, and the mean and median number of pixels per illumination (group) are also shown. The median values are linearly interpolated between the integer values of events per group.

Several features of pixel splitting become clear through a review of Figure B2. 1) The mean number of events per group are far larger than the actual source size for all source sizes and thresholds. 2) The impact of pixel splitting is the greatest for the small and medium-sized sources, ranging between factors of about 2–3. 3) Threshold has a surprisingly large effect on the distribution shape for the large source, likely due to the spatial spread of the normally distributed light source. 4) The interpolated medians are closer to the actual source sizes, particularly for the high-threshold cases. 5) Finally, the percentage of events per group with only one event is always an underestimate of the percentage of sources that are smaller than a single pixel, even for the high-threshold conditions.

These findings shed new light on the interpretation of the events-per-group histograms and statistics in Figure 8 in the paper. First, the true percentage of sources smaller than a LIS pixel is greater than the percentages in the first "bin" in Figure 8 (39% for the first 6 ms (initial breakdown), and 25% late in mature, long flashes). Second, the interpolated median of 1.5 events per group during initial breakdown is an extreme upper-bound in the typical source size early in the flash, but this upper-bound increases by a factor of 2/3 (to 2.5) late in long-duration flashes.

Acknowledgments
We are very grateful for the helpful suggestions and comments provided by William Koshak, Phillip Bitzer, Hugh Christian, Ron Holle, Doug Mach, Scott Rudlosky, Mason Quick, and by Lockheed Martin staff Samantha Edgington and Clemens Tillier. The authors acknowledge NOAA and NASA's Global Hydrology Resource Center (GHRC) for providing GLM and LIS data, respectively. LMA data were graciously provided by Jennifer Wilson, Robert Brown (NASA) and Bill Rison. Co-author (KLC) gratefully acknowledges access to the NLDN data provided by Vaisala. We also acknowledge the three anonymous reviewers for providing many useful comments. This study is funded by NASA Cooperative Agreement 80MSFC17M0022 and Air Force Contract FA252117P0046. The GLM dataset may be obtained from NOAA through the AWS s3 server at noaa-goes16.s3.amazonaws.com/index.html#GLM-L2-LCFA/ or NOAA Comprehensive Large Array-data Stewardship System (CLASS) at https://www.bou.class.noaa.gov/saa/products/welcome. The TRMM LIS dataset may be obtained from at https://ghrc.nsstc.nasa.gov/home/. The NLDN dataset can be obtained by NOAA employees and contractors at https://www.ncei.noaa.gov/data/restricted/national-lightning-detection-network/archive/. All other users must obtain the NLDN data from the data owner, Vaisala Corporation, through their host web site: https://www.corelogic.com/products/lightning-verification.aspx or by contacting brooke.pearson@vaisala.com. The LMA data used in this study is available through NASA's GHRC at https://dx.doi.org/10.5067/LMA/DATA101.

References

Bitzer, P. M. (2019). Fruit Basket of GLM Detection Efficiency. Paper presented at 2019 GLM Annual Science Team Meeting, Huntsville, Alabama.

Blakeslee, R. J. (1998). Lightning Imaging Sensor (LIS) on TRMM Science Data. NASA Global Hydrology Center Distributed Active Archive Center. https://doi.org/10.5067/LIS/LIS/DATA201

Blakeslee, R. J., Mach, D. M., Virst, K. S., Lin, A., & Buechler, D. E. (2018). Lightning Imaging Sensor (LIS) on the International Space Station (ISS): Path to Attaining Level 1 Science Requirements and Early Results in Year One, Paper presented at ISS R&D Conference, San Francisco, CA.

Boccippio, D. J., Cummins, K. L., Christian, H. J., & Goodman, S. J. (2001). Combined satellite-and surface-based estimation of the intracloud–cloud-to-ground lightning ratio over the continental United States. *Monthly Weather Review*, *129*(1), 108–122. https://doi.org/10.1175/1520-0493(2001)129<0108:CSASBE>2.0.CO;2

Boccippio, D. J., Koshak, W. J., & Blakeslee, R. J. (2002). Performance assessment of the optical transient detector and lightning imaging sensor. Part I: Predicted diurnal variability. *Journal of Atmospheric and Oceanic Technology*, *19*, 1318–1332. https://doi.org/10.1175/1520-0426(2002)019<1318:PAOTOT>2.0.CO;2

Bruning, E. C., & MacGorman, D. R. (2013). Theory and observations of controls on lightning flash size spectra. *Journal of the Atmospheric Sciences*, *70*(12), 4012–4029. https://doi.org/10.1175/JAS-D-12-0289.1

Bruning, E. C., Rust, W. D., MacGorman, D. R., Biggerstaff, M. I., & Schuur, T. J. (2010). Formation of charge structures in a supercell. *Monthly Weather Review*, *138*(10), 3740–3761. https://doi.org/10.1175/2010MWR3160.1

Bruning, E. C., & Thomas, R. J. (2015). Lightning channel length and flash energy determined from moments of the flash area distribution. *Journal of Geophysical Research: Atmospheres*, *120*, 8925–8940. https://doi.org/10.1002/2015JD023766

Cecil, D. J., Buechler, D. E., & Blakeslee, R. J. (2014). Gridded lightning climatology from TRMM-LIS and OTD: Dataset description. *Atmospheric Research*, *135*, 404–414. https://doi.org/10.1016/j.atmosres.2012.06.028

Cecil, D. J., Buechler, D. E., & Blakeslee, R. J. (2015). TRMM LIS climatology of thunderstorm occurrence and conditional lightning flash rates. *Journal of Climate*, *28*(16), 6536–6547. https://doi.org/10.1175/JCLI-D-15-0124.1

Chmielewski, V. C., & Bruning, E. C. (2016). Lightning mapping Array flash detection performance with variable receiver thresholds. *Journal of Geophysical Research: Atmospheres*, *121*, 8600–8614. https://doi.org/10.1002/2016JD025159

Christian, H. J., R. J. Blakeslee, S. J. Goodman, & Mach, D. M. (2000). Algorithm theoretical basis document for the lightning imaging sensor (NASA Earth Science Department Technical Report). Huntsville, AL.

Cummins, K. L. (2019). Full Domain Validation Using GLD360. Paper presented at 2019 GLM Annual Science Team Meeting, Huntsville, Alabama.

Cummins, K. L., & Murphy, M. J. (2009). An overview of lightning locating systems: History, techniques, and data uses, with an in-depth look at the US NLDN. *IEEE Transactions on Electromagnetic Compatibility*, *51*(3), 499–518. https://doi.org/10.1109/TEMC.2009.2023450

Franklin, V. (2013). An Evaluation of the Lightning Imaging Sensor with New Insights on the Discrimintation of Lightning Flash and Stroke Detectability, (Master Thesis). University of Alabama-Huntsville.

Fuchs, B. R., Bruning, E. C., Rutledge, S. A., Carey, L. D., Krehbiel, P. R., & Rison, W. (2016). Climatological analyses of LMA data with an open-source lightning flash-clustering algorithm. *Journal of Geophysical Research: Atmospheres*, *121*, 8625–8648. https://doi.org/10.1002/2015JD024663

Goodman, S. J., Blakeslee, R. J., Koshak, W. J., Mach, D., Bailey, J., Buechler, D., et al. (2013). The GOES-R geostationary lightning mapper (GLM). *Atmospheric Research*, *125*, 34–49. https://doi.org/10.1016/j.atmosres.2013.01.006

Goodman, S. J., Christian, H. J., & Rust, W. D. (1988). A comparison of the optical pulse characteristics of intracloud and cloud-to-ground lightning as observed above clouds. *Journal of Applied Meteorology*, *27*(12), 1369–1381. https://doi.org/10.1175/1520-0450(1988)027<1369:ACOTOP>2.0.CO;2

Hilburn, K., B. Fuchs, & Rutledge, S. A. (2019). Evaluation of GOES-16 GLM to lightning mapping arrays. Paper Presented at 99th American Meteorological Society Annual Meeting, Phoenix, AZ.

Koshak, W. J. (2010). Optical characteristics of OTD flashes and the implications for flash-type discrimination. *Journal of Atmospheric and Oceanic Technology*, *27*(11), 1822–1838. https://doi.org/10.1175/2010JTECHA1405.1

Koshak, W. J. (2011). A mixed exponential distribution model for retrieving ground flash fraction from satellite lightning imager data. *Journal of Atmospheric and Oceanic Technology*, *28*, 475–492. https://doi.org/10.1175/2010JTECHA1438.1

Koshak, W. J. (2017). Lightning NOx estimates from space-based lightning imagers. Paper Presented at Community Modeling and Analysis System Conference, Chapel Hill, NC.

Koshak, W. J., D. M. Mach, M. Bateman, P. Armstrong, & Virts, K. (2018). Product performance guide for data users, available at: https://www.ncdc.noaa.gov/data-access/satellite-data/goes-r-series-satellites#GLM

Koshak, W. J., & Solakiewicz, R. J. (2015). A method for retrieving the ground flash fraction and flash type from satellite lightning mapper observations. *Journal of Atmospheric and Oceanic Technology*, *32*(1), 79–96. https://doi.org/10.1175/JTECH-D-14-00085.1

Light, T. E., Suszcynsky, D. M., & Jacobson, A. R. (2001). Coincident radio frequency and optical emissions from lightning, observed with the FORTE satellite. *Journal of Geophysical Research*, *106*(D22), 28,223–28,231. https://doi.org/10.1029/2001JD000727

Lojou, J-Y. & Cummins, K. L..(2005). On the representation of two- and three-dimensional total lightning information. Proceedings. Paper presented at 85th American Meteorological Society annual meeting, San Diego, CAL

Mach, D. (2019). Science and operational Geostationary Lightning Mapper cluster algorithms comparison. Paper Presented at American Geophysical Union Fall Meeting, San Francisco, California.

Mach, D. M. (2020). Geostationary Lightning Mapper clustering algorithm stability. *Journal of Geophysical Research: Atmospheres*, *125*, e2019JD031900. https://doi.org/10.1029/2019JD031900

Mach, D. M., Christian, H. J., Blakeslee, R. J., Boccippio, D. J., Goodman, S. J., & Boeck, W. L. (2007). Performance assessment of the optical transient detector and lightning imaging sensor. *Journal of Geophysical Research*, *112*, 1318–1332. https://doi.org/10.1175/1520-0426(2002)019<1318:PAOTOT>2.0.CO;2

Marchand, M., Hilburn, K., & Miller, S. D. (2019). Geostationary Lightning Mapper and Earth Networks Lightning Detection over the Contiguous United States and Dependence on Flash Characteristics. *Journal of Geophysical Research: Atmospheres*, *124*, 11,552–11,567. https://doi.org/10.1029/2019JD031039

Mecikalski, R. M., Bitzer, P. M., & Carey, L. D. (2017). Why flash type matters: A statistical analysis. *Geophysical Research Letters*, *44*, 9505–9512. https://doi.org/10.1002/2017GL075003

Mecikalski, R. M., & Carey, L. D. (2018). Radar reflectivity and altitude distributions of lightning as a function of IC, CG, and HY flashes: Implications for LNOx production. *Journal of Geophysical Research: Atmospheres*, *123*, 12,796–12,813. https://doi.org/10.1029/2018JD029263

Murphy, M., & Nag, A. (2015). Cloud lightning performance and climatology of the US based on the upgraded US National Lightning Detection Network. Paper Presented at Seventh Conference on the Meteorological Applications of Lightning Data, Phoenix, Arizona.

Nag, A., M. J. Murphy, K. L. Cummins, A. E. Pifer, & Cramer, J. A. (2014). Recent Evolution of the U.S. National lightning detection network. Paper presented at 23rd International. Lightning Detection Conference, Tucson, Arizona.

Rudlosky, S. D., Goodman, S. J., Virts, K. S., & Bruning, E. C. (2019). Initial geostationary lightning mapper observations. *Geophysical Research Letters*, *46*, 1097–1104. https://doi.org/10.1029/2018GL081052

Said, R. (2019). Exploration of spatiotemporal patters of GLM flash DE using Vaisala Lightning data. Paper presented at 2019 GLM Annual Science Team Meeting, Huntsville, Alabama.

Thomas, R. J., Krehbiel, P. R., Rison, W., Hamlin, T., Boccippio, D. J., Goodman, S. J., & Christian, H. J. (2000). Comparison of ground-based 3-dimensional lightning mapping observations with satellite-based LIS observations in Oklahoma. *Geophysical Research Letters*, *27*(12), 1703–1706. https://doi.org/10.1029/1999GL010845

Thomas, R. J., Krehbiel, P. R., Rison, W., Hunyady, S. J., Winn, W. P., Hamlin, T., & Harlin, J. (2004). Accuracy of the lightning mapping array. *Journal of Geophysical Research*, *109*, D14207. https://doi.org/10.1029/2004JD004549

Thomas, R. J., P. R. Krehbiel, W. Rison, D. R. MacGorman, E. C. Bruning, & Stanley, M. A. (2019). Evaluation of the GOES-R geostationary lightning mapper (GLM) using ground-based lightning mapping Array (LMA) observations. Presented at 99th American Meteorological Society Annual Meeting, Phoenix, Arizona.

Thomason, L. W., & Krider, E. P. (1982). The effects of clouds on the light produced by lightning. *Journal of the Atmospheric Sciences*, *39*(9), 2051–2065. https://doi.org/10.1175/1520-0469(1982)039<2051:TEOCOT>2.0.CO;2

Ushio, T., Heckman, S., Driscoll, K., Boccippio, D., Christian, H., & Kawasaki, Z. I. (2002). Cross-sensor comparison of the lightning imaging sensor (LIS). *International Journal of Remote Sensing*, *23*(13), 2703–2712. https://doi.org/10.1080/01431160110107789

Yoshida, R. (2019). GLM product evaluation using ground-based lightning detection networks. Paper presented at 2019 GLM Annual Science Team Meeting, Huntsville, Alabama.

Zhang, D. (2019). Inter-Comparison of Space- and Ground-Based Observations of Lightning, (Doctoral Dissertation), University of Arizona.

Zhang, D., K. L. Cummins, & Bitzer, P. M. (2017). Ground-and Space-based Observations of Horizontally-extensive Lightning Flashes. Paper Presented at American Geophysical Union Fall Meeting, New Orleans, Louisiana.

Zhang, D., Cummins, K. L., Bitzer, P. M., & Koshak, W. J. (2019). Evaluation of the performance characteristics of the lightning imaging sensor. *Journal of Atmospheric and Oceanic Technology*, *36*(6), 1015–1031. https://doi.org/10.1175/JTECH-D-18-0173.1

Zhang, D., K. L. Cummins & Nag, A. (2015). Assessment of cloud lightning detection by the US National Lightning Detection Network using video and lightning mapping Array observations. Paper Presented at 95th American Meteorological Society Annual Meeting, Phoenix, AZ.

Zhu, Y., Rakov, V. A., Tran, M. D., & Nag, A. (2016). A study of National Lightning Detection Network responses to natural lightning based on ground truth data acquired at LOG with emphasis on cloud discharge activity. *Journal of Geophysical Research: Atmospheres*, *121*, 14,651–14,660. https://doi.org/10.1002/2016JD025574